Journal of Hazardous Materials 198 (2011) 347–355

Contents lists available at SciVerse ScienceDirect

Journal of Hazardous Materials

journal homepage: www.elsevier.com/locate/jhazmat

Cytotoxicity of serum protein-adsorbed visible-light photocatalytic Ag/AgBr/TiO_2 nanoparticles

Ji Hye Seo[a], Won Il Jeon[b], Uuriintuya Dembereldorj[a], So Yeong Lee[b,*], Sang-Woo Joo[a,*]

[a] Department of Chemistry, Soongsil University, Seoul 156-743, South Korea
[b] Laboratory of Pharmacology, College of Veterinary Medicine and Research Institute for Veterinary Science, Seoul National University, Seoul 151-742 Korea

ARTICLE INFO

Article history:
Received 14 June 2011
Received in revised form
23 September 2011
Accepted 21 October 2011
Available online 25 October 2011

Keywords:
Photocytotoxicity
Ag/AgBr/TiO_2 nanoparticles
Visible-light photocatalysts
Mitochondrial activity

ABSTRACT

Photocytotoxicity of visible-light catalytic Ag/AgBr/TiO_2 nanoparticles (NPs) was examined both *in vitro* and *in vivo*. The Ag/AgBr/TiO_2 NPs were prepared by the deposition–precipitation method. Their crystalline structures, atomic compositions, and light absorption property were examined by X-ray diffraction (XRD) patterns, X-ray photoelectron (XPS) intensities, and ultraviolet-visible (UV–vis) diffuse reflectance spectroscopic tools. The Ag/AgBr/TiO_2 NPs appeared to be well internalized in human carcinoma cells as evidenced by transmission electron microscopy (TEM). The cytotoxicity of cetylmethylammonium bromide (CTAB) appeared to be significantly reduced by adsorption of serum proteins in the cellular medium on the NP surfaces. Two types of human cervical HeLa and skin A431 cancer cells were tested to check their viability after the cellular uptake of the Ag/AgBr/TiO_2 NPs and subsequent exposure to an illumination of visible light from a 60 W/cm^2 halogen lamp. Fluorescence images taken to label mitochondria activity suggest that the reactive oxygen species should trigger the photo-destruction of cancer cells. After applying the halogen light illumination for 50–250 min and ~8 ppm (μg/mL) of photocatalytic Ag/AgBr/TiO_2 NPs, we observed a 40–60% selective decrease of cell viability. Ag/AgBr/TiO_2 NPs were found to eliminate xenograft tumors significantly by irradiating visible light *in vivo* for 10 min.

1. Introduction

Titanium dioxide (TiO_2)-based materials are one of the most promising photocatalysts used in the degradation of environmental pollutants [1]. Although TiO_2 nanoparticles (NPs) have been reported to be less toxic than other metal oxide NPs [2], there have been a number of reports studying the toxicity of TiO_2-based materials to human health and the environment [3–6]. The broad and wide employment of TiO_2 has to be however limited by its large band gap of 3.0–3.2 eV in the UV region. There have been several reports that the UV light can damage cancer cells or DNA repair processes with the use of TiO_2 [7–11]. There have been several reports about cancer-killing ability of TiO_2 using UV-light [12–14].

The necessity of UV light hampers its practical and safe use, despite TiO_2 being one of the most promising photocatalysts. The disadvantages of UV light are that it does not deeply penetrate human tissues and that it does not have a continuous prolonged cancer-killing effect [15]. To overcome these intrinsic drawbacks, a number of studies have been conducted about visible-light utilization by either impregnation [16] or metallization [17]. Some studies have been designed using the deposition of noble metals [18–21]. Recently, silver halide (AgBr) was used in a visible-light photocatalyst for the decomposition of organic species in the gas phase [22]. It has been demonstrated that AgBr on TiO_2 support is the main photoactive species in the destruction of the bacteria under visible light [23,24].

Toxicity of NPs is not well understood due to complex interactions between nano-bio interfaces [25]. Surfaces of NPs that are in contact with a biological milieu of cell culture media are expected to be in a dynamic exchange with biomolecules such as proteins [26]. Such protein adsorptions on metal oxide NPs were found to influence cytotoxicity [27]. Referring to the fact that the cationic surfactants such as cetylmethylammonium bromide (CTAB) is cytotoxic [28,29], it may be significant to estimate the reduction of cytotoxicity of NPs via serum protein adsorption. Since Ag NPs are reportedly toxic depending on the extracellular substances [30], it is interesting how the Ag-incorporated photocatalyst NPs should show the cytotoxicity behaviors under visible light illumination.

Despite several reports about the ability of Ag/AgBr/TiO_2 to kill bacteria [23,24], it remains unclear to the best of the authors' knowledge, how the photocytotoxicity of NPs could be estimated using only visible light. Considering that the used CTAB for the synthesis of Ag/AgBr/TiO_2 NPs is cytotoxic, it has not yet been

* Corresponding authors. Tel.: +82 2 8200434; fax: +82 2 8790378.
E-mail addresses: leeso@snu.ac.kr (S.Y. Lee), sjoo@ssu.ac.kr (S.-W. Joo).

0304-3894/$ – see front matter © 2011 Elsevier B.V. All rights reserved.
doi:10.1016/j.jhazmat.2011.10.059

ascertained whether these NPs may kill the mammalian cells via a visible photocatalytic process after interacting with the cellular medium. In the present work, we study the feasibility of selective photo-induced killing of cells using the visible-light photocatalyst NPs. For this purpose we used Ag/AgBr/TiO_2 NPs for selective damage of HeLa and A431 cancer cells by controlling their concentration and halogen light illumination time.

2. Materials and methods

2.1. Preparation of NPs and physical characterization

Ag/AgBr/TiO_2 NPs were prepared by the deposition–precipitation method. A 1 g quantity of P-25 TiO_2 (Ovonyx, U.S.A.) was added to 100 mL of distilled water, and the suspension was sonicated using a Saehan SH-2140 sonicator (1.2 A, 190 W) at 28 kHz for 30 min. Then, 1.2 g of CTAB (Sigma, 99.0%) was added to the suspension, and the mixture was stirred magnetically for 30 min, then 0.21 g of $AgNO_3$ in 2.3 mL of NH_4OH (28–30 wt% NH_3, Sigma–Aldrich) was quickly added to the mixture. In this process, at alkaline condition, cationic surfactant CTAB could adsorb onto the surface of TiO_2 to limit the number of nucleation sites for the AgBr metal island to grow, leading to homogeneously dispersed AgBr. The resulting suspensions were stirred at room temperature for 12 h. The product was either filtered using a 0.2 μm Satorius Stedim Biotech ministart syringe filter or centrifuged at 3000 ppm for 5 min, washed with water, and dried at 70 °C. Finally, the powder was calcined in air at 500 °C for 3 h. UV–vis reflectance spectrum of the Ag/AgBr/TiO_2 NP powder was taken using a JASCO V-670 spectrophotometer equipped with an ISN-723 integral sphere accessory. XRD patterns were observed by Rigaku Miniflex X-ray diffractometer. XPS spectra were observed at a X-ray take-off angle at 56° by a VG microtech ESCA 2000 instrument under the vacuum of 10^{-9} Torr using a Al Ka source (14.086.6 eV).

The infrared spectra were obtained using a thermoelectron 6700 Fourier-transform infrared spectrometer with a nominal resolution of 4 cm^{-1} and 256 scanning times. A portion of the powdered sample was transferred onto a DiffuseIR heated chamber (Pike Technologies). High-resolution transmission electron microscopy (TEM) images were obtained using a JEOL JEM-3010 microscope at an accelerage voltage of 100–300 kV.

2.2. Cell culture and uptake of NPs in cancer cells

HeLa (human cervical carcinoma) cells were grown on DMEM in a steri-cycle CO_2 incubator (Thermo Fisher Scientific), whereas A431 (human epidermoid carcinoma) cells were cultured on RPMI 1640. All cells were supplemented with 10% fetal bovine serum (FBS) and 1% penicillin–streptomycin antibiotics (Gibco)/0.2 ppm plasmocin and maintained in 5% CO_2/95% humidified air at 37 °C. Approximately 10^5–10^6 cells were washed with phosphate buffer saline and 0.25% trypsin–EDTA was added for 3 min to detach the

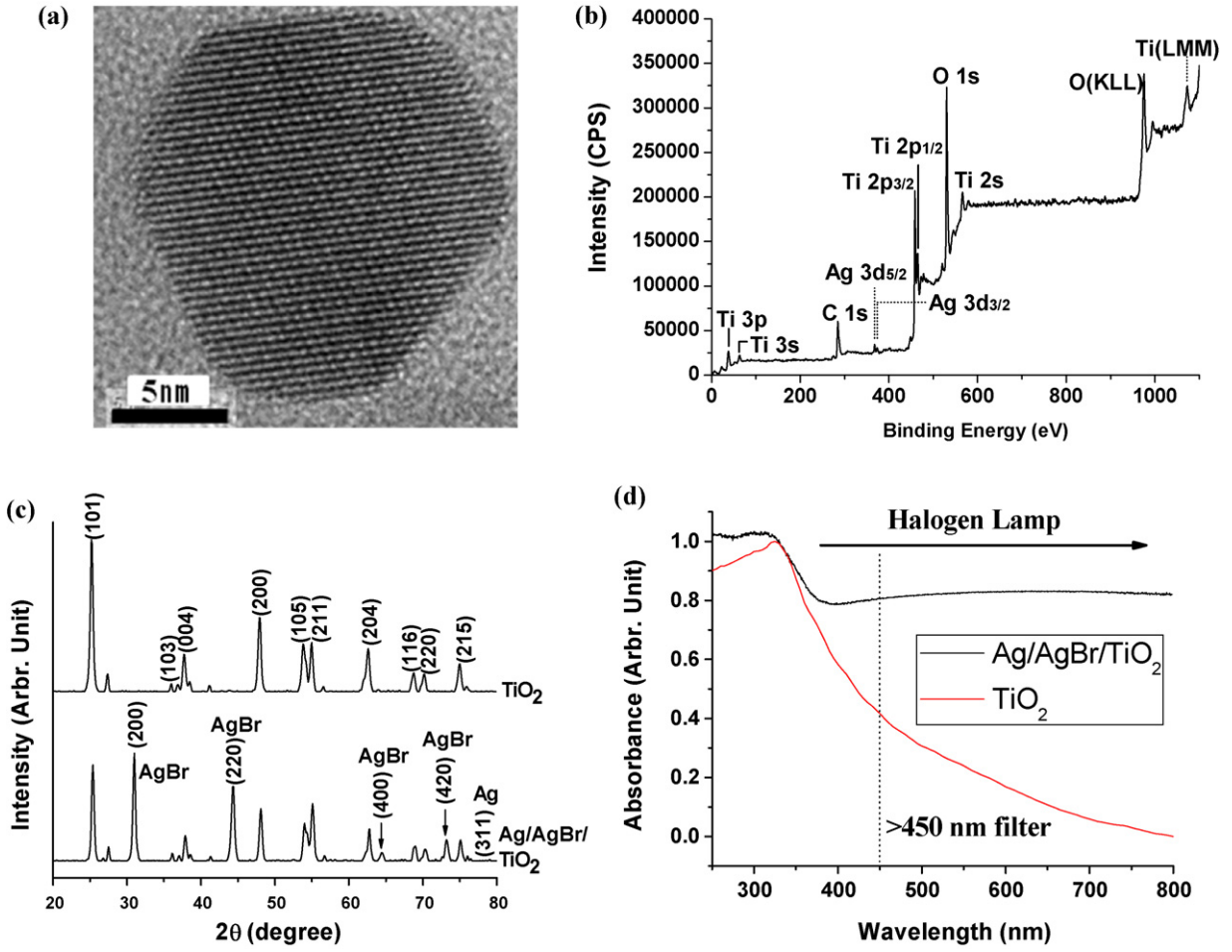

Fig. 1. (a) HR-TEM image, (b) XPS, (c) XRD, and (d) UV–vis reflectance spectra of Ag/AgBr/TiO_2 NPs. For TiO_2, the crystal planes of strong anatase peaks were indicated in the XRD spectrum with the omission of the weak rutile peaks. The absorption spectrum of pure P25 TiO_2 NPs in ethanol is also compared.

cells and counted by a hematocytometer. Dulbecco's phosphate buffered saline (DPBS) was used to wash seeded cells. The cells were seeded at the confocal dish and placed in an incubator at a maintained temperature of 37 °C overnight. A live cell chamber (Model: Chamlide TC) was purchased from LCI instruments. Cell viability was also tested using a CCK-8 assay (Dojindo, Japan).

2.3. TEM, optical, and fluorescence images of NPs in cancer cells

The uptake of Ag/AgBr/TiO_2 NPs was examined using TEM. A431 cells were plated on a 100 mm culture dish (SPL, Korea) at a concentration of 1×10^4 cells per dish containing growth medium before the cells were exposed to the NPs. NPs were added, and the cells were incubated at 37 °C with 5% CO_2. After 24 h, the cells were washed twice with DPBS, fixed in Karnovsky's fixative for 24 h, and post-fixed in 0.05 M of osmium tetroxide. (En bloc staining at 4 °C for overnight.) After fixation, specimens were rinsed with and dehydrated in a graded series of 30, 50, 70, 80, 90% ethanol and three times in 100% ethanol, for 10 min each. (The transition treatment solution remained at room temperature for 15 min, and was centrifuged at 1200 rpm for three minutes. This procedure was repeated two times.) Samples were embedded in a mixture of resin in propylene oxide polymerized at 70 °C. Ultrathin sections for TEM measurements were prepared with a diamond knife. Samples were analyzed using a JEOL JEM-1010 microscope at an accelerate voltage of 40–100 kV. Cellular uptake of NPs was also monitored using a conventional optical microscopy. An Olympus IX-71 inverted microscope was employed with a high sensitive CCD camera (CoolSnap HQ2, Roper Scientific). An objective lens (×40 or ×60) with a corrected thickness for the cover glass was used to obtain the image using the CCD camera. MitoTtracker orange (Product No. M7510) was purchased from Invitrogen (Carlsbad, USA). A filter set of 510–550 nm excitation, 570 nm dichroic, and 575 (±12.5) nm emission filters from Semrock (Rochester, USA) was used to obtain the fluorescence images. Mitochondrial activities of its fluorescence marker were estimated quantitatively using a BD FACScalibur flow cytometer. A 100 W halogen bulb (Philips Model No. 7724, USA) was used to irradiate the cell samples with a focused area of 1.33 cm^2. A long-pass filter (Cat. No. 10LWF-450-B) from Newport (Irvine, USA) was used to cut-off the UV illumination below 450 nm with transmission efficiency over 80%. We apply CCK-8, propylium iodide cytotoxicity assays. Cytotoxicity was tested using the tryphan blue test [live cell/(live cell + dead cell)] × 100%. A trypan blue staining kit (Cat. No: 15250-061) was purchased from GIBCO (Carlsbad, USA). The number of cells was counted by a hemacytometer for the viability test. The isolated cells (2×10^6) were then injected into the back of nude mice (ages 4–6 wk) for a xenograft model. A volume of 40 μL of the prepared Ag/AgBr/TiO_2 NPs (~100 ppm) was injected to the tumor. An *in vivo* irradiation experiment was performed with an approximately 60 W/cm^2 irradiation for 10 min using an Eurosep spot.il.5180 fiber optic illuminator (Christophe, France). The isolated cells (2×10^6) were then injected into the back of nude mice (CAnN.Cg-Foxn1^{nu}/CrljOri, ages 4–6 wk, male) for a xenograft model. As controls, we used either NPs or light free. A volume of 40 μL of the prepared Ag/AgBr/TiO_2 NPs (~100 ppm) was injected to the tumor. An *in vivo* irradiation experiment was performed with approximately 60 W/cm^2 for 10 min using an Eurosep spot.il.5180 fiber optic illuminator (Christophe, France). The volume of tumor was evaluated using the formula volume = (width × length × depth) × (π/6). The initial concentration of 100 ppm for *in vivo* experiments became diluted in the tumor. Considering the initial average tumor size value of 307 (±19) mm^3 (3.07×10^{-7} m^3) and the initial volume 40 μL (4.0×10^{-8} m^3) of the injected NP solution, the final concentration of $AgAgBrTiO_2$ NPs in the tumor could be estimated as low as 13.0 ppm. Also it has to be mentioned that the particles were incubated for as long as 24 h, whereas we irradiated only for 10 min after injecting the NPs for *in vivo* experiments.

3. Results and discussion

3.1. Physical characterization

Fig. 1(a) and (b) shows the HR-TEM image and X-ray photoelectron microscopy (XPS) spectrum of Ag/AgBr/TiO_2 NPs. Fig. 1(c) illustrates the XRD patterns of the catalysts. The calcined photocatalyst displayed crystalline reflection peaks that are characteristic of the anatase and rutile TiO_2 and AgBr. The samples exhibited the common anatase and rutile phases of P-25 TiO_2. The two major diffraction peaks at 31° and 44° attributed to the (2 0 0) and (2 2 0) crystal planes of AgBr were observed for the Ag/AgBr/TiO_2 samples [18] amongst the strong anatase peaks of TiO_2 [31]. The other two (4 0 0) and (4 2 0) AgBr peaks were also found in the XRD spectrum. The weakness of the Ag X-ray diffraction peaks is due to a low atomic percentage of Ag in $AgAgBrTiO_2$ NPs. The concentration of Ag is reported 1.35–3.41% from the previous report [24]. Our XPS spectrum of $AgAgBrTiO_2$ NPs also supports that the Ag content is relatively smaller than other species as presented in Fig. 1(b). In addition, the peaks of Ag(1 1 1) at 38.1°, Ag(2 0 0) at 44.3°, and Ag(2 2 0) at 64.4° were overlapped with the strong TiO_2 and AgBr peaks. Although it was not magnified, we could manage to identify the weak feature correspond to Ag(3 1 1) at 77.5° in the XRD

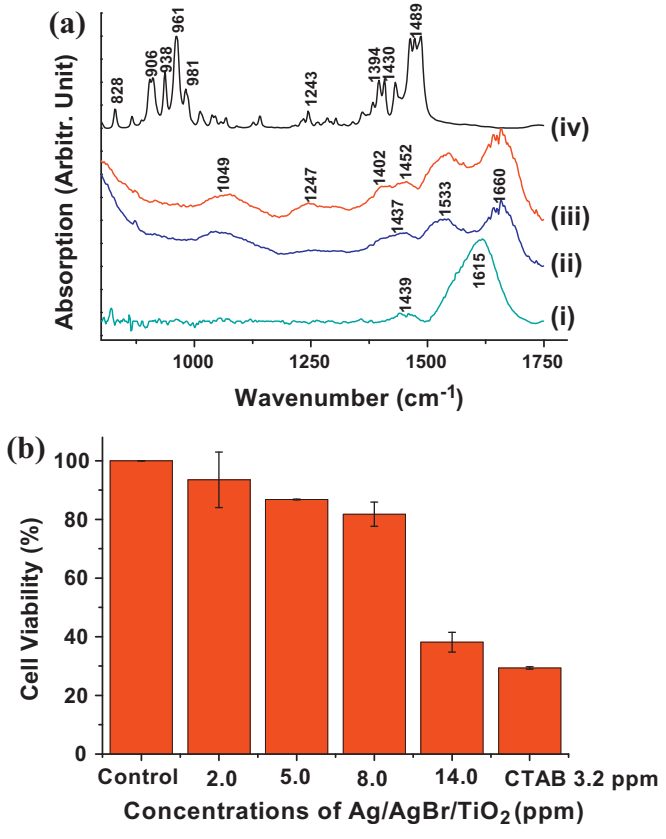

Fig. 2. (a) Infrared spectra of serum protein capped Ag/AgBr/TiO_2 NPs in comparison with CTAB and TiO_2 NPs. Diffuse reflectance infrared spectra of Ag/AgBr/TiO_2 NPs (i) before and after coating, (ii) the DMEM and (iii) RPMI cell culture media containing 10% FBS solution. Solid infrared spectrum of CTAB is included in (iv) for a better comparison. (b) CCK-8 assay of Ag/AgBr/TiO_2 NPs concentrations in the range of 2.0, 5.0, 8.0, and 14.0 ppm in A431 cells. The toxicity of CTAB (3.2 ppm) is also compared with that of 8 ppm of Ag/AgBr/TiO_2 NPs.

spectrum. As shown in Fig. 1(d), the UV–vis reflectance spectra of Ag/AgBr/TiO_2 NPs showed a substantial visible light absorption band between 400 and 800 nm due to the indirect band gap or the surface plasmon absorption of silver, differing from the case of TiO_2. However, it should be mentioned that the Ag/AgBr/TiO_2 NPs have a strong absorption peak between 200 and 400 nm ascribed to the direct band gap of AgBr overlaid by the strong absorption peak at 380 nm (3.2 eV) of anatase TiO_2. This strong UV absorption may affect the cell damage despite the weakness of the halogen lamp at this region as suggested by the following data about killing of photo-induced cancer cells. Although the absorption band of pure P25 TiO_2 NPs fell sharply around at 400 nm, a weak absorption was found at this wavelength region as shown in Fig. 1(d). We chose to use a cut-off filter of a longer wavelength above 450 nm instead of that above 400 nm to test the wavelength region where pure P25 TiO_2 NPs could not significantly influence.

3.2. Cellular uptake of Ag/AgBr/TiO_2 NPs into HeLa and A431 cells after adsorption of serum proteins

Fig. 2(a)(i) shows the infrared spectra of Ag/AgBr/TiO_2 NPs after adsorption of serum proteins in cell culture media. In fact the infrared spectrum of Ag/AgBr/TiO_2 NPs at Fig. 2(a)(i) showing its water adsorption peaks [32] did not match with the CTAB peaks [33]. The spectra became similar to the protein bands [34] after adsorption on both the DMEM and RPMI cellular medium containing the serum proteins of FBS (10%.) as shown in Fig. 2(a)(ii) and (iii). Since we cannot correlate any CTAB peaks in Fig. 2(a)(iv) after the treatment of the cellular media, it is likely that the Ag/AgBr/TiO_2 NPs exhibits different characteristics from CTAB in itself. Fig. 2(b) shows CCK-8 analysis of Ag/AgBr/TiO_2 NPs concentrations; 2.0 ppm, 5.0 ppm, 8.0 ppm, and 14.0 ppm. The toxicity of 3.2 ppm of CTAB is also compared at the last column. This toxicity is estimated to be higher than that contained in 8.0 ppm of Ag/AgBr/TiO_2 NPs. It was found that the toxicity of CTAB reduced for Ag/AgBr/TiO_2 NPs significantly presumably after adsorption of the proteins.

Fig. 3 shows the TEM images of Ag/AgBr/TiO_2 NPs in HeLa and A431 cells. The TEM images clearly show the particle load inside the cells. The endosome (or lysosome) encapsulation of Ag/AgBr/TiO_2 NPs suggests a receptor-mediated endocytosis presumably after adsorption of the serum proteins. We found that both HeLa and A431 cells showed similar behaviors. After confirming that the two types of human carcinoma HeLa and A431 cells can uptake the visible-light photocatalyst NPs after adsorption of serum proteins with alleviation of the CTAB toxicity,

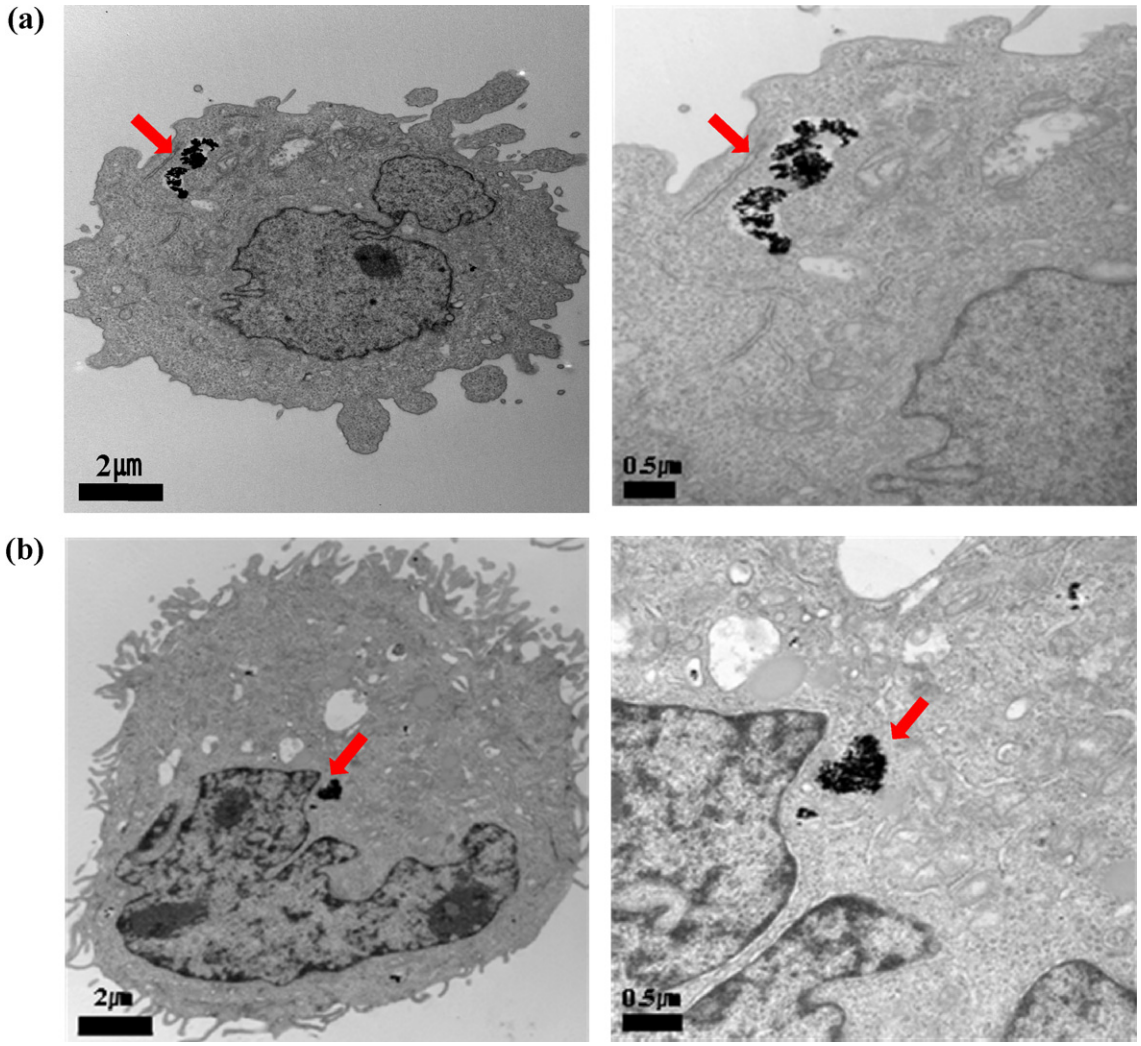

Fig. 3. TEM image of (a) HeLa and (b) A431 cells after the uptake of Ag/AgBr/TiO_2 NPs. Images on the right are magnified views of those on the left. The arrows indicate the locations of internalized NPs.

we performed the photoinduced killing of cancer cells using the Ag/AgBr/TiO_2 NPs. We have found that it usually takes 24 h for the cellular uptake of NPs without any cell targeting groups from the TEM data. After ensuring that the NPs were inside the cells, we performed the photo-induced cytotoxicity experiments after the pre-treatment.

3.3. Photo-induced damages of HeLa and A431 cells by a halogen lamp

Fig. 4 shows optical microscopy images of the viability test of HeLa cells treated with or without Ag/AgBr/TiO_2 NPs under halogen light illumination. Morphological changes of cells seen in the

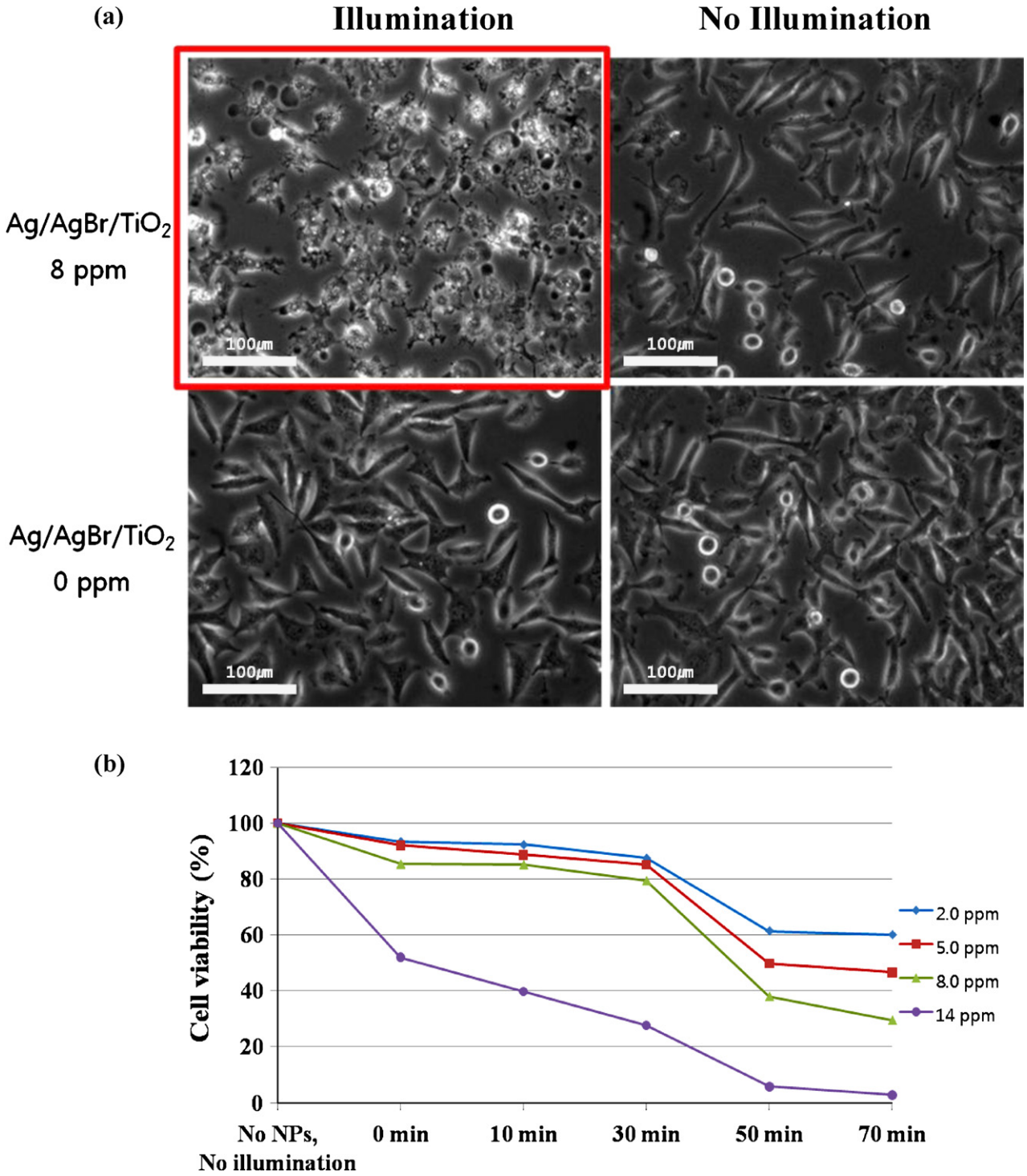

Fig. 4. (a) Optical inverted phase-contrast microscopy images for viability of HeLa cells treated with Ag/AgBr/TiO_2 NPs incubated for longer than 24 h. The upper left: ~8 ppm of NPs under halogen light illumination in the presence of the long-pass UV-cut-off filter (>450 nm) for 250 min. The upper right: ~8 ppm of NPs in the absence of halogen light. The lower left: halogen light illumination in the presence of the long-pass UV-cut-off filter (>450 nm) for 250 min without NPs. The lower right: no illumination without NPs. Viability of HeLa cells as a function of halogen light illumination time. (b) The trypan blue exclusion test. The cells were treated with different Ag/AgBr/TiO_2 NPs concentrations in the range of 2.0, 5.0, 8.0, and 14.0 ppm. It shows a consistent tendency that the cell viability is affected depending on the irradiation time and concentrations of Ag/AgBr/TiO_2 NPs under our experimental conditions. The NPs were incubated for 24 h prior to the light exposure experiments.

optical microscopy images may provide information about the $Ag/AgBr/TiO_2$ photocatalytic effects. It was found that HeLa cells are substantially damaged by the treatment of ~8 ppm (μg/mL) of $Ag/AgBr/TiO_2$ NPs when illuminated by halogen light with the UV cut-off filter for 250 min.

We performed a cancer cell viability experiment by illuminating a 60 W/cm^2 halogen lamp. Since the cells were in a temperature-controlled live-cell chamber, the thermal heating effect was not expected to be significant and only the photo-induced damages should be the main cause of the cell death under our experimental conditions. We checked viability of HeLa cells as a function of halogen light illumination time. The cells were treated with different $Ag/AgBr/TiO_2$ NPs concentrations; 2.0 ppm, 5.0 ppm, 8.0 ppm, and 14.0 ppm using trypan blue measurements. Fig. 4(b) shows a consistent tendency that the cell viability is affected depending on the irradiation time and concentrations of $Ag/AgBr/TiO_2$ NPs under our experimental conditions.

As shown in Fig. 5(a), the effects of halogen light illumination in the absence of $Ag/AgBr/TiO_2$ NPs on cells were insignificant, while the halogen light illumination in the presence of $Ag/AgBr/TiO_2$ NPs proved to kill the cancer cells effectively. With the concentration of $Ag/AgBr/TiO_2$ NPs (~8 ppm), a majority of the cancer cells (>60%) were killed in 50 min of halogen light exposure. At a concentration of ~8 ppm, the significant cell death was not observed without the illumination. A431 cells also exhibited similar behaviors as shown in Fig. 5(b) except they were irradiated for 110 min. Fig. 5(c) shows stick diagrams for a comparative viability test of HeLa and A431 cells. If either the irradiating light or the $Ag/AgBr/TiO_2$ NPs were absent, the cell damage was considerably reduced and the viability could reach up to ~80% as shown in Fig. 5. By applying the halogen lamp light after the treatment of $Ag/AgBr/TiO_2$ photocatalytic NPs, we observed up to a ~60% decrease in cell viability. Our results indicated that controlled cancer cell killing can be conducted by changing the duration of exposure to specific concentrations of the $Ag/AgBr/TiO_2$ NPs.

As indicated by Fig. 5, we observed a phenomenal decrease of cell viability particularly for A431 cells after the halogen light illumination even without $Ag/AgBr/TiO_2$ NPs. This was presumably due to the weak UV light strength from the halogen lamp. A long-pass cut-off filter (>450 nm) can provide the benefit of avoiding the cellular damage due to the UV light. Since the halogen lamp has non-negligible light intensity of 350–450 nm in the UV-region [35] where the $Ag/AgBr/TiO_2$ NPs have strong absorption, it is possible that the halogen light alone might damage the cells. The illumination energy curve of our halogen lamp suggests that our halogen lamp has approximately 5–20% intensity at 350 nm in the UV light in comparison with that at 500 nm in the visible region at a temperature range between 2800 and 3400 K. If the temperature is below 2600 K, there is almost no intensity at 350–400 nm in the UV region. Considering that the $Ag/AgBr/TiO_2$ NPs have a stronger absorption at ~350 nm, the possibility of the UV light-induced cell damage cannot be completely eliminated without the long-pass filter ($\lambda > 450$ nm). Fig. 5(c) shows the viability test in the presence of the long-pass UV-cut-off filter (>450 nm) for 250 min. It should be mentioned that a longer illumination time for 250 min was necessary if the long-pass filter was introduced. Even in the presence of the filter, the cell viability decreased slightly by ~5%, indicating the visible-light-induced damage. This decrease was not however as significant as the data without the filter as shown in Fig. 5(b). The cell viability also increased from ~40% to ~60% after introducing the filter. Fig. 5(c) summarizes the viability data with the filter ($\lambda > 450$ nm). It is quite similar to the data in Fig. 5(a). One of the advantages lies in the fact that the UV light-induced damages can be completely eliminated by introducing the filter. It was found that the cells without NPs under the illumination equipped with the filter were also slightly damaged with ~5%, presumably due to longer illumination time, as shown in Fig. 5. TiO_2 NPs appeared to exhibit different cytotoxicities depending on cell lines from the previous report [36]. The different irradiation time conditions required to damage the cancer cells for the two cell lines may be explained in their dissimilar cytotoxicities under out experimental conditions. Effective cancer cell killing could be achieved with our experimental set-up by controlling the concentrations of visible-light photocatalyst NPs and the duration of the halogen light exposure time.

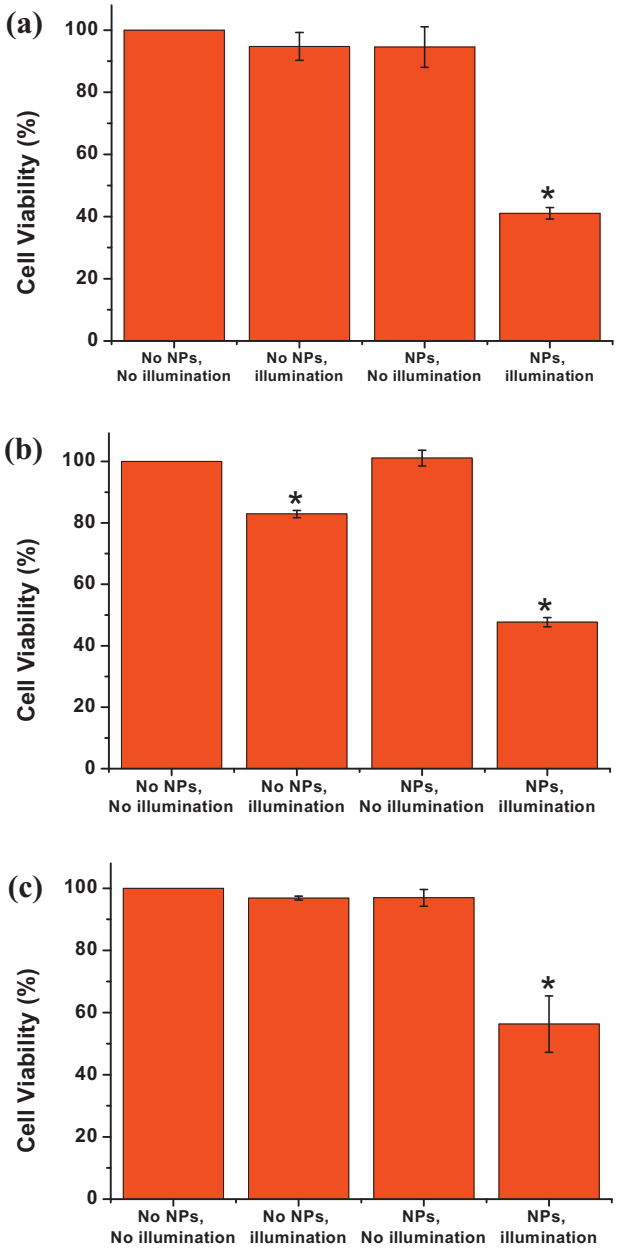

Fig. 5. Trypan blue exclusion test of cell viability. Comparison of viability of (a) HeLa cells irradiated for 50 min and (b) A431 cells irradiated for 100 min treated with $Ag/AgBr/TiO_2$ NPs incubated for longer than 24 h into the cells. (c) Comparison of viability of HeLa cells treated with $Ag/AgBr/TiO_2$ NPs incubated for longer than 24 h after the addition of NPs to the cells in the presence of the long-pass UV-cut-off filter (>450 nm) for 250 min. Statistical analysis of the data was performed by a one-way analysis of variance (*t*-test). *Significant difference $p < 0.05$. Statistical analysis of the data was performed by a one-way analysis of variance (*t*-test). *Significant difference $p < 0.05$.

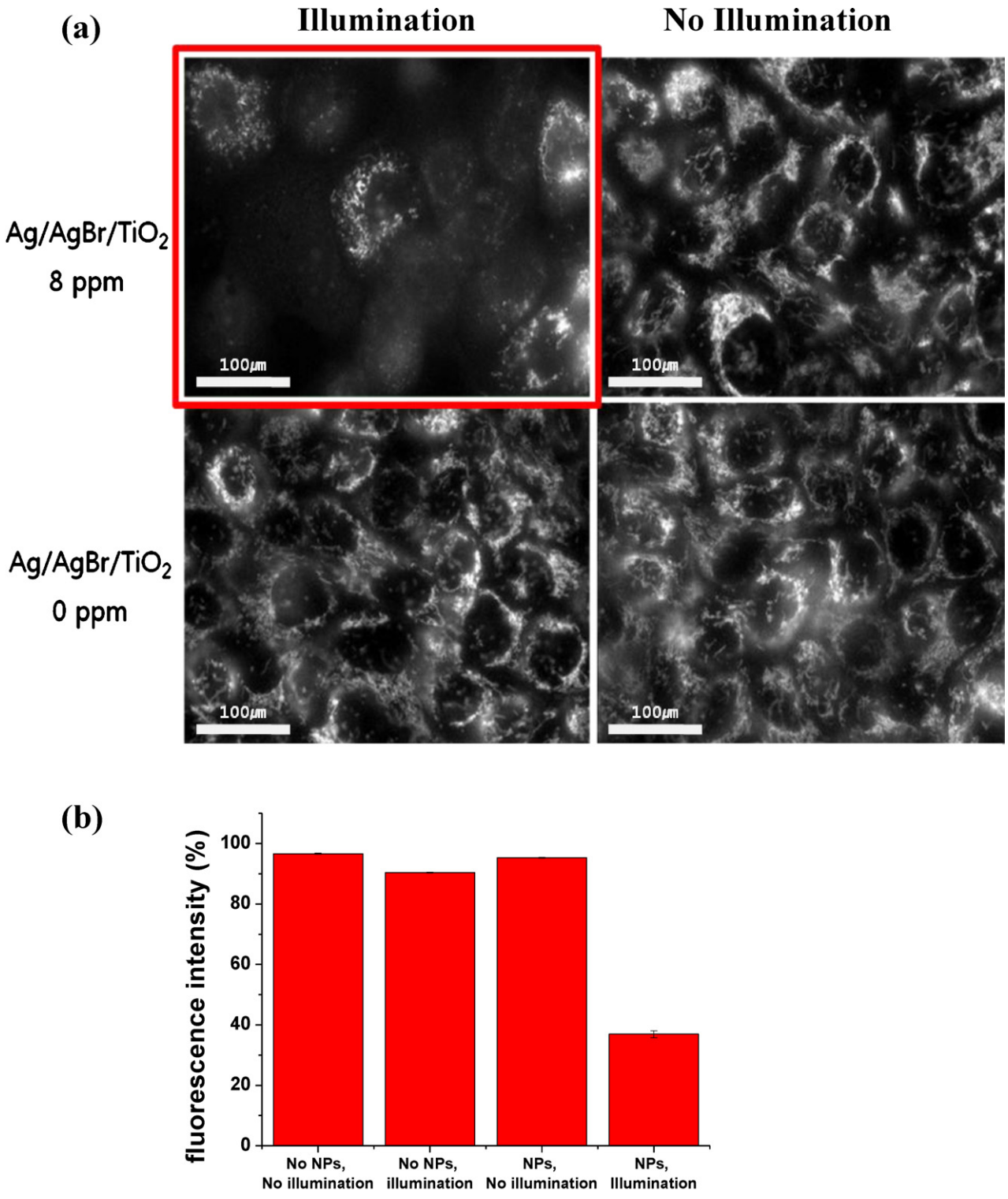

Fig. 6. (a) Mitochondrial activity in A431 cells. The upper left: fluorescence images for visualization of mitochondrial activity after treatment of ~8 ppm of Ag/AgBr/TiO_2 NPs under halogen light illumination for 50 min. The fluorescence intensity of mitochondria, stained with MitoTracker orange was measured. Scale bars: 100 μm. The upper right: ~8 ppm of NPs in the absence of halogen light. The lower left: halogen light illumination for 50 min without NPs. The lower right: no illumination, no NPs. (b) Plot of mitochondrial activities depending on Ag/AgBr/TiO_2 NPs and visible irradiation. The error bars indicate the standard deviations of three independent measurements.

3.4. Cell destruction mechanisms: reactive oxygen species (ROS)

The photocatalytic cancer cell killing mechanism should be caused by the reactive oxygen species. It was found that Ag/AgBr/TiO_2 NPs could be slightly toxic in themselves even without the illumination. Fig. 6 shows the photoinduced destruction mechanism by visualizing mitochondrial activity after NP treatment of ~8 ppm (μg/mL) in A431 cells. Increased intracellular ROS generation triggers activation of defense mechanisms to restore radical balance in the cell. These processes can be assessed by mitochondrial activity. Microscopic examination of mitochondria was used to compare their activity amongst cell samples. After

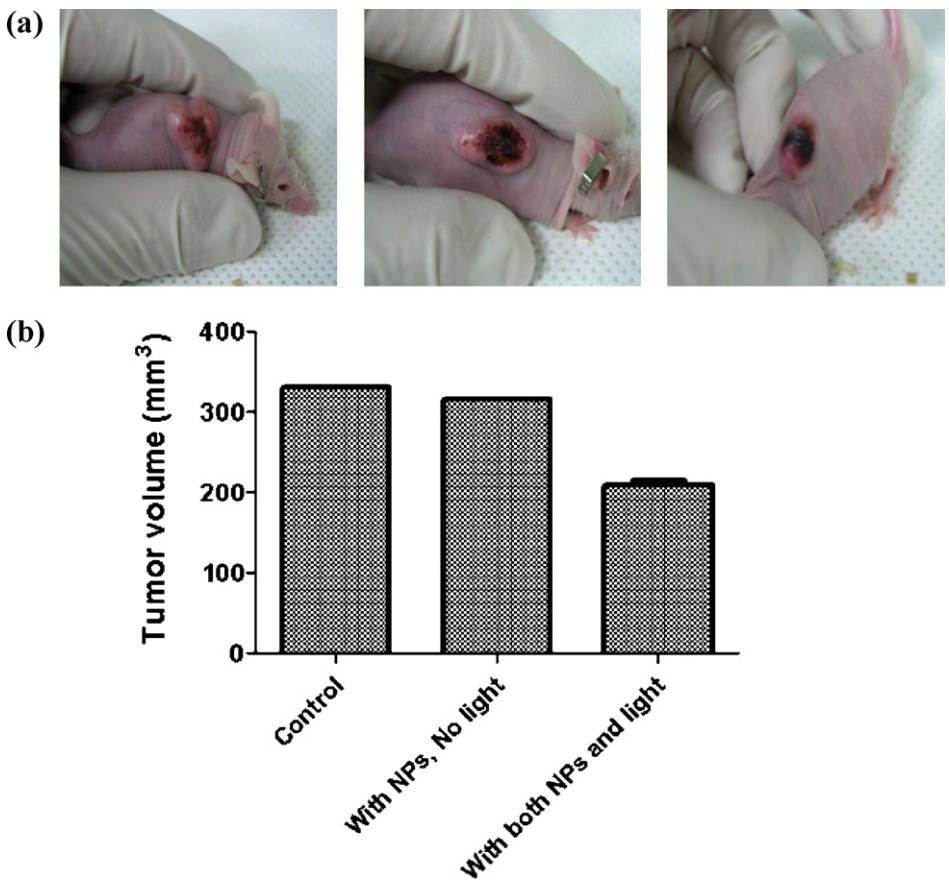

Fig. 7. (a) Photographs of A431-xenograft tumor on mice in the absence of NPs and irradiation for 10 min (left), in the presence of NPs without irradiation (middle), and in the presence of both NPs and irradiation for 10 min (right). (b) Stick diagrams of the measured tumor volumes (mm^3) for the three types of samples.

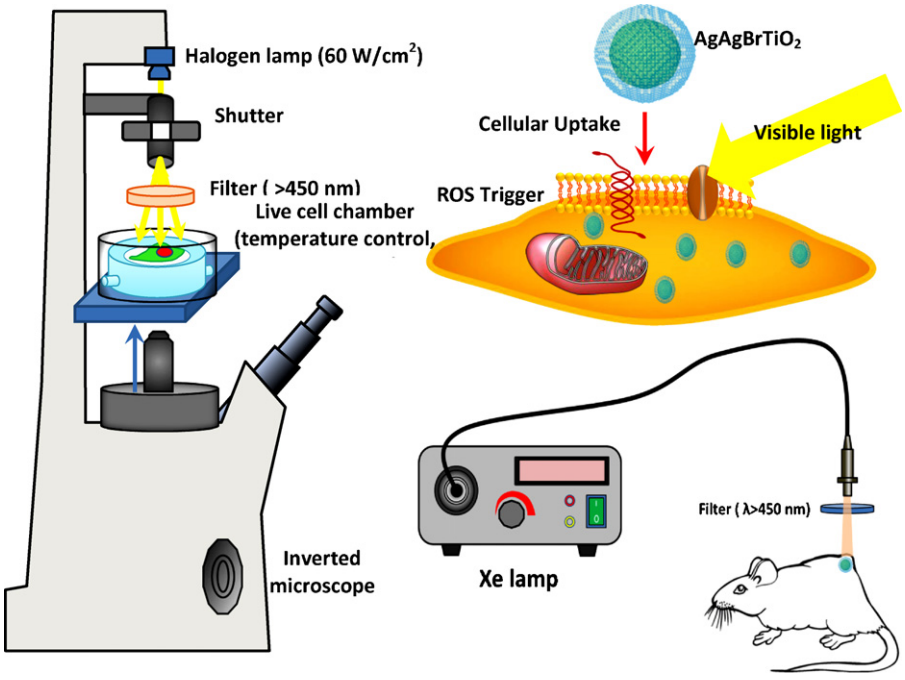

Fig. 8. Schematic diagram of the experimental set-up for visible illumination to human carcinoma cells embedded in a live-cell chamber and an *in vivo* set-up. Plausible cell killing mechanism by visible-light photocatalysts is also listed.

treatment with Ag/AgBr/TiO_2 NPs at 8 ppm, the mitochondrial fluorescence intensity became decreased by ~40% than that of the controls. An independent fluorescence activated cell sorting (FACS) measurement also supported that the decrease in fluorescence intensity for mitochondrial activities should be ascribed with Ag/AgBr/TiO_2 NPs and visible irradiation, as shown in Fig. 6(b).

3.5. *In vivo experiment*

Fig. 7(a) shows the photographs of *in vivo* experimental results suggesting the photoinduced tumor destruction. Fig. 7(b) shows a stick diagram of tumor sizes of A431-xenograft tumor on mice in the absence of NPs and irradiation, in the presence of NPs without irradiation, and in the presence of both NPs and irradiation. HeLa cell-xenografted tumor on mice shows similar results although not shown. Fig. 8 illustrates our experimental schematic diagram for visible illumination to human carcinoma cells embedded in a live-cell chamber and *in vivo* experiments using Ag/AgBr/TiO_2 NPs.

4. Conclusions

In this work, we report selective viability reduction behaviors of visible-light photocatalyst Ag/AgBr/TiO_2 NPs in HeLa and A431 cancer cells using a halogen light source without any UV interference. Internalized Ag/AgBr/TiO_2 NPs can induce the killing of mammalian cancer cells above a specific concentration and an illumination time. Such photo-induced cell damage was not identical for the two cell lines in terms of illumination time. When the cut-off filter transmitting above 450 nm was introduced between the halogen light source and the cell culture dish embedded in a CO_2-supplied and temperature-controlled live-cell chamber, we observed damages to human carcinoma cells for the Ag/AgBr/TiO_2 NP-treated samples in a discriminating way without any interference from UV light. Our result suggests that Ag/AgBr/TiO_2 NPs can be substantially photocytotoxic for *in vitro* and *in vivo* cell damages even in the absence of UV-light damages.

Acknowledgement

This research was supported by the Basic Science Research Program through the National Research Foundation of Korea (NRF) funded by the Ministry of Education, Science, and Technology (2011-0001316, 2011-0027696) and the Development of Characterization Techniques for Nano-materials Safety Project of KRCF. S-W. J would like to thank Dr. Keunchang Cho and Prof. Sung Ik Yang for valuable comments.

References

[1] K.Y. Foo, B.H. Hameed, Decontamination of textile wastewater via TiO_2/activated carbon composite materials, Adv. Colloid Interface Sci. 159 (2010) 130–143.
[2] P. Kocbek, K. Teskac, M.E. Kreft, J. Kristl, Toxicological aspects of long-term treatment of keratinocytes with ZnO and TiO_2 nanoparticles, Small 6 (2010) 1908–1917.
[3] J.R. Peralta-Videa, L. Zhao, M.L. Lopez-Moreno, G. de la Rosa, J. Hong, J.L. Gardea-Torresdey, Nanomaterials and the environment: a review for the biennium 2008–2010, J. Hazard. Mater. 186 (2011) 1–15.
[4] K.V. Thomas, J. Farkas, E. Farmen, P. Christian, K. Langford, Q. Wu, K.E. Tollefsen, Effects of dispersed aggregates of carbon and titanium dioxide engineered nanoparticles on rainbow trout hepatocytes, J. Toxicol. Environ. Health A 74 (2011) 466–477.
[5] C.W. Dunnill, I.P. Parkin, Nitrogen-doped TiO_2 thin films: photocatalytic applications for healthcare environments, Dalton Trans. 40 (2011) 1635–1640.
[6] L. Reijnders, Hazard reduction for the application of titania nanoparticles in environmental technology, J. Hazard. Mater. 152 (2008) 440–445.
[7] V.T. DeVita, T.S. Lawrence, S.A. Rosenberg, Cancer, Wolters Kluwer, Lippincott Williams and Wilkins, Philadelphia, USA, 2008.
[8] H.M. McGee, G.M. Woods, B. Bennett, R.S. Chung, The two faces of metallothionein in carcinogenesis: photoprotection against UVR-induced cancer and promotion of tumour survival, Photochem. Photobiol. Sci. 9 (2010) 586–596.
[9] R. Guo, J. Chen, F. Zhu, A.K. Biswas, T.R. Berton, D.L. Mitchell, D.G. Johnson, E2F1 localizes to sites of UV-induced DNA damage to enhance nucleotide excision repair, J. Biol. Chem. 285 (2010) 19308–19315.
[10] A.J. Callegari, E. Clark, A. Pneuman, T.J. Kelly, Postreplication gaps at UV lesions are signals for checkpoint activation, Proc. Natl. Acad. Sci. U.S.A. 107 (2010) 8219–8224.
[11] L. Dong, J. Wen, E. Pier, X. Zhang, B. Zhang, F. Dong, N. Ziegler, M. Mysz, R. Armenta, R. Cui, Melanocyte-stimulating hormone directly enhances UV-Induced DNA repair in keratinocytes by a xeroderma pigmentosum group A-dependent mechanism, Cancer Res. 70 (2010) 3547–3556.
[12] Q. Li, X. Wang, X. Lu, H. Tian, H. Jiang, G. Lv, D. Guo, C. Wu, B. Chen, The incorporation of daunorubicin in cancer cells through the use of titanium dioxide whiskers, Biomaterials 30 (2009) 4708–4715.
[13] Y. Chihara, K. Fujimoto, H. Kondo, Y. Moriwaka, T. Sasahira, Y. Hirao, H. Kuniyasu, Anti-tumor effects of liposome-encapsulated titanium dioxide in nude mice, Pathobiology 74 (2007) 353–358.
[14] E.A. Rozhkova, I. Ulasov, B. Lai, N.M. Dimitrijevic, M.S. Lesniak, T.A. Rajh, A high-performance nanobio photocatalyst for targeted brain cancer therapy, Nano Lett. 9 (2009) 3337–3342.
[15] S. Rehman, R. Ullah, A.M. Butt, N.D. Gohar, Strategies of making TiO_2 and ZnO visible light active, J. Hazard. Mater. 170 (2009) 560–569.
[16] L. Wang, J. Mao, G-H. Zhang, M.J. Tu, Nano-cerium-element-doped titanium dioxide induces apoptosis of Bel 7402 human hepatoma cells in the presence of visible light, World J. Gastroenterol. 13 (2007) 4011–4014.
[17] P. Wang, B. Huang, X. Qin, X. Zhang, Y. Dai, M-H. Whangbo, Ag/AgBr/WO(3)·H(2)O: visible-light photocatalyst for bacteria destruction, Inorg. Chem. 48 (2009) 10697–10702.
[18] M. Bowker, D. James, P. Stone, R. Bennett, N. Perkins, L. Millard, J. Greaves, A. Dickinson, Catalysis at the metal–support interface: exemplified by the photocatalytic reforming of methanol on Pd/TiO_2, J. Catal. 217 (2003) 427–433.
[19] T.G. Schaaff, D.A. Blom, Deposition of Au-nanocrystals on TiO_2 crystallites, Nano Lett. 2 (2002) 507–511.
[20] B. Sun, A.V. Vorontsov, P.G. Smirniotis, Role of platinum deposited on TiO_2 in phenol photocatalytic oxidation, Langmuir 19 (2003) 3151–3156.
[21] P. Wang, B. Huang, X. Zhang, X. Qin, H. Jin, Y. Dai, Z. Wang, J. Wei, J. Zhan, S. Wang, J.G. Wang, M.-H. Whangbo, Highly efficient visible-light plasmonic photocatalyst Ag@AgBr, Chem. Eur. J. 15 (2009) 1821–1824.
[22] S. Rodrigues, S. Uma, I.N. Martyanov, K.J. Klabunde, Decontamination of gaseous acetaldehyde over CoOx-loaded SiO_2 xerogels under ambient, dark conditions, J. Catal. 233 (2005) 405–410.
[23] M.R. Elahifard, S. Rahimnejad, S. Haghighi, M.R. Gholmai, Apatite-coated Ag/AgBr/TiO(2) visible-light photocatalyst for destruction of bacteria, J. Am. Chem. Soc. 17 (2007) 9552–9553.
[24] C. Hu, Y. Lan, J. Qu, X. Hu, A. Wang, Ag/AgBr/TiO_2 visible light photocatalyst for destruction of azodyes and bacteria, J. Phys. Chem. B 110 (2006) 4066–4072.
[25] I. Lynch, A. Salvati, K.A. Dawson, Protein–nanoparticle interactions: what does the cell see? Nat. Nanotechnol. 4 (2009) 546–547.
[26] Z. Ji, X. Jin, S. George, T. Xia, H. Meng, X. Wang, E. Suarez, H. Zhang, E.M. Hoek, H. Godwin, A.E. Nel, J.I. Zink, Dispersion and stability optimization of TiO_2 nanoparticles in cell culture media, Environ. Sci. Technol. 44 (2010) 7309–7314.
[27] M. Horie, K. Nishio, K. Fujita, S. Endoh, A. Miyauchi, Y. Saito, H. Iwahashi, K. Yamamoto, H. Murayama, H. Nakano, N. Nanashima, E. Niki, Y. Yoshida, Protein adsorption of ultrafine metal oxide and its influence on cytotoxicity toward cultured cells, Chem. Res. Toxicol. 22 (2009) 543–553.
[28] R.G. Rayavarapu, W. Petersen, L. Hartsuiker, P. Chin, H. Janssen, F.W. van Leeuwen, C. Otto, S. Manohar, T.G. van Leeuwen, In vitro toxicity studies of polymer-coated gold nanorods, Nanotechnology 21 (2010) 145101.
[29] A.M. Alkilany, P.K. Nagaria, C.R. Hexel, T.J. Shaw, C.J. Murphy, M.D. Wyatt, Cellular uptake and cytotoxicity of gold nanorods: molecular origin of cytotoxicity and surface effects, Small 5 (2009) 701–708.
[30] C.O. Dimkpa, A. Calder, P. Gajjar, S. Merugu, W. Huang, D.W. Britt, J.E. McLean, W.P. Johnson, A.J. Anderson, Interaction of silver nanoparticles with an environmentally beneficial bacterium, *Pseudomonas chlororaphis*, J. Hazard. Mater. 188 (2011) 428–435.
[31] G.B. Shan, G.P. Demopoulos, The synthesis of aqueous-dispersible anatase TiO_2 nanoplatelets, Nanotechnology 21 (2010) 025604.
[32] P.A. Connor, K.D. Dobson, A.J. McQuillan, Infrared spectroscopy of the TiO_2/aqueous solution interface, Langmuir 15 (1999) 2402–2408.
[33] S. Xing, Y. Chu, X. Sui, Z. Wu, Synthesis and characterization of polyaniline in CTAB/hexanol/water reversed micelle, J. Mater. Sci. 40 (2005) 215–218.
[34] M.E. Lee, S.Y. Lee, S.W. Joo, K.H. Cho, Amide I bands of terminally blocked alanine (Ac-Ala-NHMe) in solutions investigated by infrared spectroscopy and density functional theory calculation: hydrogen-bonding interactions and solvent effects, J. Phys. Chem. B 113 (2009) 6894–6897.
[35] G.R. Hopkinson, T.M. Goodman, S.R. Prince, A Guide to the Use and Calibration of Detector Array Equipment, SPIE Press, Bellingham, WA, USA, 2004.
[36] S.K. Sohaebuddin, P.T. Thevenot, D. Baker, J.W. Eaton, L. Tang, Nanomaterial cytotoxicity is composition, size, and cell type dependent, Part. Fibre Toxicol. 7 (2010) 22.